Earth ArXiv

This version is a preprint submitted to EarthArXiv and has not yet undergone peer review.

Local Seismicity: Matched Filter Detection Routine with Synthetic Templates using 1D velocity model

Eva Káldy * [1], **Tomáš Fischer** [1], **Jana Doubravová** [2]

[1]Institute of Hydrogeology, Engineering Geology and Applied Geophysic, Faculty of Science, Charles University, Albertov 6, Prague, 120 00, Czech Republic, [2]Geofyzikální ústav Akademie věd ČR, v. v. i., Boční II/1401, 141 00 Prague 4 – Spořilov, Czech Republic

Author contributions: *Conceptualization*: Eva Káldy. *Methodology*: Eva Káldy. *Software*: Eva Káldy. *Formal Analysis*: Eva Káldy. *Resources*: Jana Doubravová, Tomáš Fischer. *Writing - Original draft*: Eva Káldy. *Writing - Review & Editing*: Eva Káldy, Tomáš Fischer. *Funding acquisition*: Tomáš Fischer.

Abstract This study evaluates the performance of Synthetic Template Matching for seismic event detection in the West Bohemia region (Czechia), comparing it with two established methods: the automated detector-locator PEPiN and Artificial Neural Network. Synthetic Templates are generated using a 1D velocity model and span a grid of five fundamental focal mechanisms (FMs), independent of any prior waveform or FM knowledge. The resulting catalog includes origin time, similarity, magnitude, location, number of detecting templates, and interpreted focal mechanism. In WEBNET data, Synthetic Template Matching with cross-correlation thresholds of 0.4 detected 264 events with completeness magnitude $M_C-0.1$. All the detected seismicity is real and local, its FMs (interpreted within the seismic network) align dominantly with the strike-slip events. Although the method does not outperform PEPiN or Artificial Neural Network in M_C, it reliably estimates focal mechanisms and epicentral locations.

Non-technical summary Match filter detection routine is a very powerful instrument allowing detecting micro-earthquakes with waveform amplitudes at and below the noise level. It requires knowledge of a template waveform, and it recognizes only the earthquakes of similar pattern - nearby location and similar focal mechanism. Therefore, this detection method is not used in regions without previously detected earthquakes. But some studies already show that Synthetic Templates are also performing well.Our research is driven by the following questions: To what level can a synthetic waveform perform as a template for a match filter detection routine? Can similarity between real event and Synthetic Template be used to estimate focal mechanism? Especially when a grid of synthetic temples is used, utilizing only five elementary focal mechanisms. Our test site is West Bohemia / Vogtland region (Czech Republic), where natural seismicity is monitored both by Artificial Neural Network and amplitude based PEPiN detector.

*Corresponding author: eva.kaldy@natur.cuni.cz

1 Introduction

The purpose of this study is to test to which level a set of Synthetic Templates can serve to detect local seismicity, with the aim of application in areas without known seismic activity, especially when monitoring potentially induced seismicity near geothermal wells (Zang et al., 2014), hydrocarbon extraction (Clarke et al., 2014; Grigoli et al., 2018), CO_2 storage (White and Foxall, 2016), or similar.

Template matching is a traditional waveform-based detection method that relies on cross-correlation (similarity) to identify seismic events. It compares continuous seismic data with waveforms of previously recorded earthquakes (templates) to reveal highly similar events that are often missed by standard detection methods, especially those near or below the typical detection threshold (Shelly et al., 2006; Janská and Eisner, 2012; Gibbons and Ringdal, 2006). Template matching has been widely applied across various spatial scales and research contexts, including the detection and analysis of fluid-induced seismicity (Shelly et al., 2013, 2016), identification of repeating earthquakes (Chamberlain et al., 2017; Janská and Eisner, 2012), and the enhancement of seismic catalogs from local (Diaferia et al., 2024; Essing and Poli, 2022) to regional scales (Ross et al., 2019). However, the classical form of template matching is limited to detecting only the seismicity with location and focal mechanism similar to a previously known seismic source. This limitation can be addressed by a linear combination of known templates (subspace detector, Harris, 1991), or by synthetic template matching (Chamberlain and Townend, 2018; Rodgers et al., 2006, this study).

For Synthetic Template Matching, Synthetic Templates are required to reflect the relative arrival time of P and S waves to the stations in order to rise the similarity at all the stations simultaneously; achieving such is not easy without knowledge of the real seismicity. The shape of the waveform can be a simple Ricker wavelet, a decaying sine (naïve synthetics in Chamberlain and Townend, 2018), or a wavelet reflecting the specific underground condition (Green's function synthetics in Chamberlain and Townend, 2018, this study); ideally, the P and S amplitudes vary at the components and stations according to the focal mechanism. The latter type of synthetic waveform (based on Greens functions) is expected to show the highest similarity to the real seismic event.

Generating realistic synthetic seismograms for the Synthetic Template Matching is a complex task, with Green's functions (GFs) at its core (Shearer, 2009). Green's functions describe Earth's response to unit impulsive point sources, encapsulating its elastic properties and boundary conditions. The process begins by defining the parameters of the seismic source, such as location, focal mechanism, and magnitude. Seismic wave propagation is then simulated using methods such as numerical modeling, ray tracing, homogeneous layering, normal modes, or semi-analytical approaches (Shearer, 2009; Wang et al., 2017), each relying on the best available structural Earth model. The spatial derivatives of the GFs are convolved with the source-time function to generate synthetic seismograms at specific stations. To further align these with real observations, instrument response and local site effects can be incorporated. In particular, when earthquakes occur near recording stations, the resulting higher-frequency content requires more detailed subsurface models for accurate simulation (Levin et al., 2010).

The velocity model determines the level to which the relative arrival time of the P and S waves will reflect the arrival of the real wave. Therefore, for Synthetic Template Matching, it would be best to use an accurate 3D velocity model, but such a model is unlikely to be available in a region where the Synthetic Template Matching detection is likely to be applied (monitoring of uprising geothermal project, etc.). The velocity model for synthetic seismograms must include not just the P and S wave velocity profile but also density and attenuation variation with depth. A geological profile and some basic geophysical measurements from the borehole are expected to be available, leading to a relatively precise 1D velocity model of the upper kilometers, more refined at the top (Káldy and Fischer, 2025). Note that if the detection method by synthetic template matching proves itself to be worthy with synthetic templates created with a 1D velocity model, its performance can only be improved by using the 3D velocity model.

There is a little difference in template matching procedure when using synthetic-waveform templates instead of the real-waveform ones: number of templates, and merging of similarities from all the stations. The number of real templates reflects the diversity of known seismicity; on the other hand, the number of Synthetic Templates reflects all the potential variation in focal mechanism, depth, and epicentral location. Second, the similarities between template and real waveforms add up in the real template scenario, when no variation in P and S wave arrivals is expected. However, synthetic seismograms are likely to exhibit a difference in arrivals between real and simulated waveforms because the velocity model is always just an approximation. Therefore, a simple stacking of components similarities might not suffice to detect a real event, and a more advanced form of stacking is needed.

This study presents a modified matched filter detection routine that utilizes Synthetic Templates. It's effectivity is tested in West Bohemia (Czech Republic, Europe, Fig. 1) on local natural seismicity ($T_p - T_s > 1$ s), with synthetic seismograms generated using a simple 1D velocity model (Málek et al., 2005; Vavryčuk et al., 2022, Tab. 1). The detection and location performance of template matching with Synthetic Templates is compared to two algorithms routinely detecting seismicity in the West Bohemia: First, the automated seismic detector and locator PEPiN (Fischer, 2003; Káldy and Fischer, 2025, Polarization based Earthquake PIcker for Networks). Second, the neural network detection (Doubravová and Horálek, 2019). Further, the similarities between Synthetic Templates and a detected event are used to estimate the focal mechanism of the event. Such focal mechanism estimates are compared to the moment tensor catalog of earthquakes in West Bohemia from 2008 to 2018 by Vavryčuk et al. (2022) which uses manual picks and relevant locations Institute of Geophysics (2024).

1.1 West Bohemia / Vogtland seismic region

The West Bohemia / Vogtland region in the Czech Republic (at the boundary with Germany, Fig. 1) is a geodynamically active area characterized by earthquake swarms, CO_2 emissions, mofette fields, and mineral springs. Geologically, it lies at the convergence of three major tectonic units: Saxothuringian, Teplá-Barrandian and the Moldanubian. Two significant fault systems define the region: the Mariánské Lázně fault, oriented northwest-southeast, and the Ore Mountains fault, oriented west-southwest to east-northeast (Vavryčuk et al., 2022). In particular, the area exhibits Tertiary and Quaternary volcanism, with the most recent volcanic activity occurring during the Holocene epoch.

Seismic activity in West Bohemia predominantly manifests itself as earthquake swarms on the NNW blind fault intersecting the NW Mariánské Lázně fault, particularly concentrated near the village of Nový Kostel (blue points in Fig. 1). These swarms consist of numerous small to moderate earthquakes ($M_L < 4.5$) that occur over short periods, typically without a single main-shock. The focal depths of these events range from 6 to 12 km. To monitor this activity, the local seismic network WEBNET was established, comprising 23 stations strategically placed around the main focal zone near Nový Kostel (Institute of Geophysics, 1991, triangles in Fig. 1). This network enables detailed mapping of the fault structures and real-time observation of seismic events, facilitating a deeper understanding of

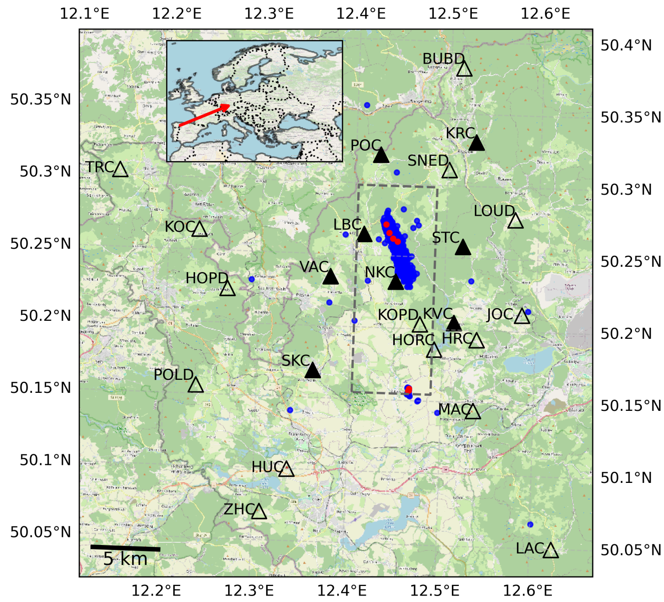

Figure 1 WEBNET is a local seismic network in the West Bohemia of the Czech Republic (at the boundary with Germany), Europe. On the map, 23 online seismic stations are pointed in triangles and station names (Institute of Geophysics, 1991, IG CAS); filled triangles is the subset of eight stations used routinely by PEPiN and in this study by the Synthetic Template Matching and Neural Network detection. An example seismic activity (Institute of Geophysics, 2024, manual locations 2018 $M > 1$ by IG CAS,) is pointed by blue points, 7 events with focal mechanisms from day 2018.138 are in red points (4 events in the North cluster, 3 overlapping in South cluster). The major North cluster seismic activity aligns NNW; it is close to stations LBC and NKC. The minor South cluster is in the southern part of WEBNET, between stations MAC and SKC. Gray dashed line - span of Synthetic Templates grid used in this study. The inset shows Europe; red arrow pointing to West Bohemia.

the region's geodynamics.

In this study only an eight-station subset of WEBNET is used (filled triangles in Fig. 1), to resemble a long-term monitoring of aseismic regions such as with planned geothermal wells, injection CO_2, or extraction of hydrocarbons. The West Bohemia/Vogtland test site presents a setting analogous to that of induced seismicity monitoring systems. The typical depths of earthquakes ($\sim$ 9 km) are comparable to the average spacing between permanent seismic stations, ensuring good coverage and detection capability of the network. The majority of seismic activity is concentrated near the center of the network (North cluster), mimicking scenarios of induced seismicity directly associated with borehole operations. In contrast, a smaller fraction of events occur outside the network perimeter (South cluster), serving as a proxy for potentially triggered seismicity in the surrounding region.

The subset of eight WEBNET stations surrounds the Nový Kostel fault zone, leaving the smaller Southern swarm outside. The eight subset stations are NKC, LBC, VAC, STC, KVC, SKC, POC, and KRC (pointed by filled triangles in Fig. 1, similar stations to Káldy and Fischer, 2023), spanning 13 km N-S and 8 km E-W. All these stations are planted with similar seismometers: broadband sensors Guralp CMG-3ESPC, sampling is 250 Hz (Institute of Geophysics, 1991, www.ig.cas.cz).

1.2 Detection methods in WEBNET

The WEBNET network is consistently monitored using two independent, fully automated methods that run in parallel, with prominent events subsequently verified and interpreted manually. As mentioned, the PEPiN system operates with 8 stations (filled triangles in Fig.1) situated around the main focal area of Nový Kostel. The data collected by these stations are processed every hour, analyzing the previous 60 minutes of continuous data to detect seismic events. PEPiN identifies the onsets of both S- and P-waves, associates them with the expected event criteria, and calculates the hypocenter location and local magnitude (Káldy and Fischer, 2025). To ensure accuracy, the algorithm requires at least four valid S-wave picks and one P-wave pick. Events with location residuals below 0.1 seconds are displayed on the website (https://www.ig.cas.cz/vyzkum-a-vyuka/observatore/lokalni-seismicka-sit-webnet/), while all events, including those with higher residuals, are stored in the internal database for future analysis.

Additionally, all waveforms are processed daily using an event detection algorithm based on Artificial Neural Networks (ANN). This method operates independently on waveforms from each station, ideally across all 23 stations, and searches for signals indicative of local seismic events, as pre-trained. The individual station-based detections are then passed through a coincidence scheme that identifies simultaneous triggers on at least 6 stations. Time periods matching these criteria are labeled events and stored in the database, with the maximum amplitude of the traces used as a preliminary indicator of potential higher magnitudes.

The outputs from both detection methods are then manually reinterpreted by seismologists. For the purpose of this study, we run the ANN detector on the eight-station configuration only, with a coincidence of five stations to declare an event.

2 Methodology & Setup: Synthetic Template Detection

The goal is to create a grid of Synthetic Templates that detects all earthquakes in the area of interest, regardless of its exact location or focal mechanism. A dense grid with great variation of focal mechanisms would serve the detection well, but the computation cost would be too high. The aim is to make the detection possible to run on a standard multi-core computer at reasonable time. Tools such as Pyrocko (Heimann et al., 2017, 2019, 2020) facilitate the generation of synthetic waveforms using established velocity models and modified ObsPy (Beyreuther et al., 2010) serves the template matching detection.

2.1 Velocity model

For Synthetic Template Matching, the realistic synthetic seismograms are the core. Such realistic seismograms can be achieved best by proper modeling and by using the best available velocity model of the region, with a specific focus on upper layers.

West Bohemia / Vogtland region has been studied for velocities, attenuation, and densities in 1D and 3D (Málek et al., 2005; Mousavi et al., 2015; Karousová et al., 2012; Fallahi et al., 2013). Since this study aims to test its usability for regions less explored than West Bohemia / Vogtland, only the 1D isotropic velocity model by Málek et al. (2005) will be used (Tab. 1, version published by Vavryčuk et al., 2022); the depth scale was adjusted to kilometers below sea level to match this project. A similar velocity model was used to determine focal mechanisms in the region of Nový Kostel (Vavryčuk et al., 2022).

Each 1D velocity model is only an approximation of the Earth's velocities, the difference from the real field being due to anisotropy, inhomogeneities, changes in porosity, chemical composition and layers thickness over the distance, etc. In West Bohemia, the study by Málek et al. (2005) shows 5% P-wave anisotropy, and variation 0 - 0.5 km/s between here used model and WB95 model (Novotný, 1996). In total, the cumulative uncertainty in the velocity model is below 10%, when the seismic source is at 10 km depth.

Depth [km]	-0.675	-0.4	-0.1	0.4	1.4	3.4	5.4	9.4	19.4	31.4
V_p [km/s]	4.30	5.06	5.33	5.60	5.87	6.09	6.35	6.74	7.05	7.25
ρ [g/cm^3]	1.7	2.2	2.3	2.5	2.5	2.5	2.6	2.6	2.6	2.9
Q_p	30	40	50	60	80	100	150	200	300	400

Table 1 1D velocity (Earth) model for West Bohemia / Vogtland: velocities and attenuation factors (Málek et al., 2005) are as published by Vavryčuk et al. (2022), and densities from Málek et al. (2005). Depth is given in kilometers above sea level. $V_p/V_s = 1.7, Q_p/Q_s = 2$.

2.2 Generating synthetic seismograms

A synthetic seismogram represents the theoretical ground motion at a given receiver location in response to a hypothetical earthquake. The generation of synthetic seismograms requires several key inputs: a defined focal mechanism, source location, magnitude, a velocity model of the subsurface, the positions of recording stations, and appropriate computational tools.

For this work, synthetic seismograms were generated at eight stations from the WEBNET network surrounding Nový Kostel (see Fig. 1) using the open-source Pyrocko toolbox developed by Heimann et al. (2017, 2019, 2020). Green's functions (GFs) were computed using Pyrocko's Fomosto module, which supports various computational backends depending on the scale and requirements of the simulation. We employed the QSEIS backend (Wang, 1999), which models wave propagation in a layered, viscoelastic half-space. Grid parameters and sampling rates are similar to Káldy and Fischer (2025), selected to prevent aliasing in both the time and spatial domains.

Based on the computed GFs, Pyrocko facilitates the simulation of both point and finite seismic sources, as well as a range of source time functions. Our simulation setup closely follows that of Káldy and Fischer (2025), with the exception that we adopt the 1D velocity model for the West Bohemia region developed by Málek et al. (2005) (see Tab. 1). To scale the synthetic waveforms, we use the moment magnitude M_W (Hanks and Kanamori, 1979); however, for comparison with observed local seismicity, results are presented in local magnitude M_L. The ground motion is modeled in terms of velocity to match the format of the recorded velocigrams.

The simulations cover a frequency band of 1–10 Hz, with emphasis placed on the lower end of the spectrum compared to Káldy and Fischer (2025). This focus is intended to mitigate the influence of small-scale heterogeneities in the subsurface. All eight WEBNET stations used in this study are equipped with broadband sensors whose response remains flat across the 1–10 Hz range (Güralp Systems Limited, 2021), enabling straightforward conversion of waveform data from digital counts to physical ground velocity in units of m/s.

2.2.1 Synthetic vs. real event

Although in a real case scenario of monitoring an aseismic region, this would not likely be an option, we choose to compare real event waveforms with synthetic ones; the synthetics being constructed with all the parameters we know about the real seismic event. The comparison in Fig. 2 reveals variations in relative S-wave arrival times ranging from 0 to 0.22 seconds. The greatest differences are observed at stations that are second closest (LBC) and second most distant (POC). Note that waveforms are scaled to match the maximum amplitudes between real and synthetic, therefore the variation in amplitude and so in the interpreted magnitudes is not pronounced here.

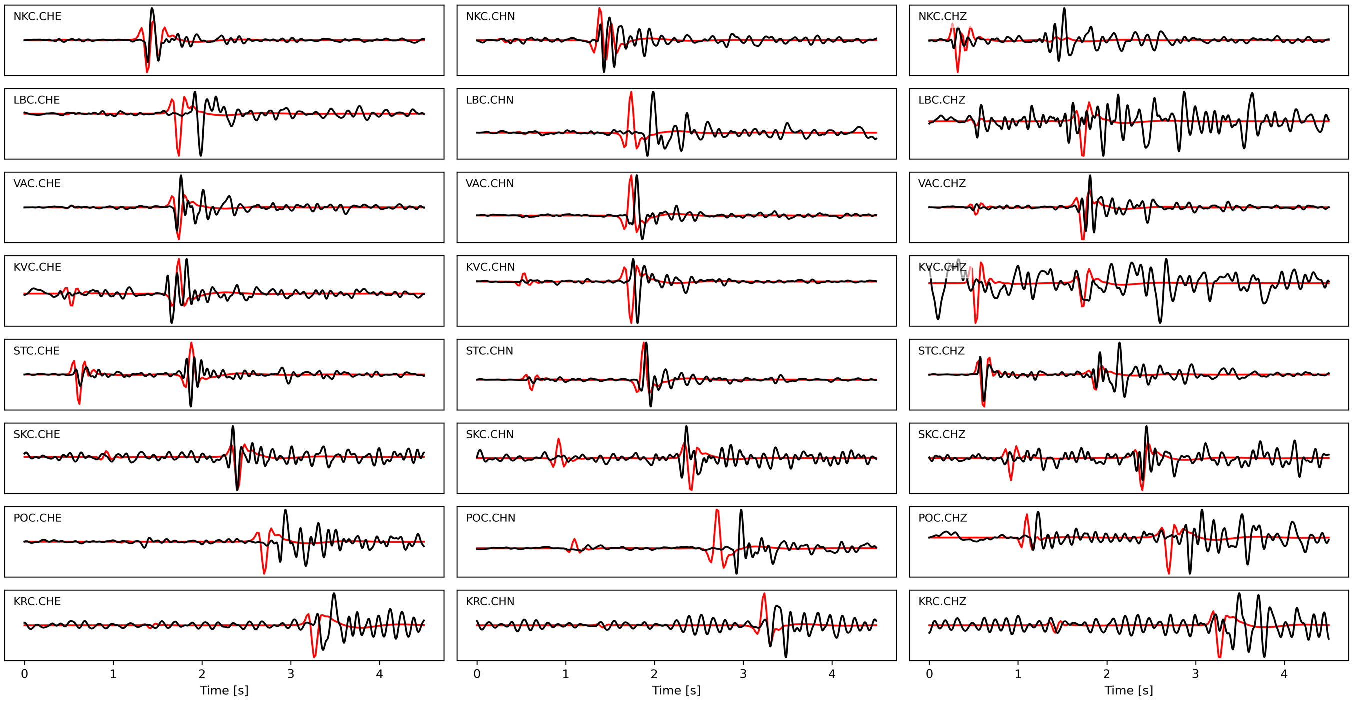

Figure 2 Real vs. Synthetic Waveforms: 2014/05/30 3:09:20, $M_L 0.55$ ($M_w 1.31$), location: N50.2266, E12.4461, depth 8.7 km; focal mechanism strike 40°, dip 57°, rake 82°. Event parameters by Vavryčuk et al. (2022). Real waveforms in black, synthetic ones in red, both bandpass filtered 1-10 Hz, scaled to match maximum waveform of a component, East component in first column, North in second, vertical component in right column. Stations in rows are ordered by the epicentral distance.

2.3 Grid of Synthetic Templates

Synthetic Template Matching detection technique is particularly well-suited for regions where enhanced detection of seismic activity is desired but empirical templates are unavailable or insufficient. To ensure effective detection, the Synthetic Templates must adequately sample all the possible variation in waveforms due to variation of source location and focal mechanism.

To cover the variation in waveforms due to the source location, the templates are calculated with the spatial extent reflecting the target area. We choose that the grid of Synthetic Templates covers the center of the station subset, extending more to the south, spanning 6 x 16 km, 7 - 11 km in the depth, resulting in total 2 975 Synthetic Templates. This grid has spacing 1 km and it covers most of the known seismic events in the area, focusing on the Northern cluster and leaving out most of the Southern seismic cluster right out of the grid. This serves as a test of the detectability for events outside the grid and outside the seismic network. The grid span is indicated by a gray dashed line in Fig. 1, red points are the automated locations by PEPiN.

To cover the possible variation in waveforms due to changes in focal mechanism, a constant variation in strike, dip and rake for each grid point would cause a dramatic increase in number of templates, but since each focal mechanism without volumetric change can be reconstructed on the basis of five double-couple focal mechanisms (Zahradník and Sokos, 2018, Fig. 3), only these five focal mechanisms are chosen for the synthetic seismograms to cover all the expected waveform modulations. See an example of resulting Synthetic Templates in Fig. 3a-e for all five representative focal mechanisms. The seismic source is at depth 8 km, 2.3 km North from the NKC station. The seismograms vary mainly in the S-to-P amplitude ratio and in the S-wave polarity at each component; some templates' components are much alike (Fig. 3: component E in b and c, component N in b and c, etc.).

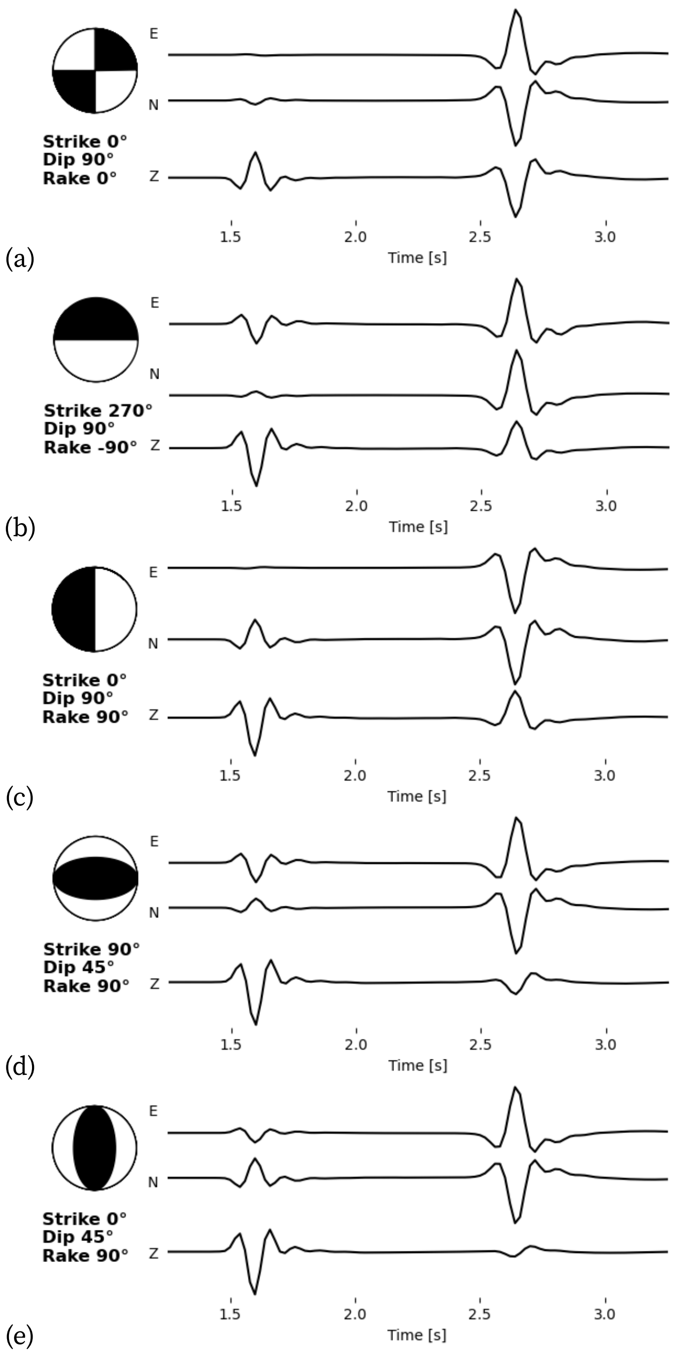

Figure 3 Synthetic Templates located 2.3 km North of the NKC station (N50.2536, E12.4461), at 8 km depth. These synthetic seismograms are created for five of six elementary moment tensors used in ISOLA (Zahradník and Sokos, 2018, Table 1) using Pyrocko (Heimann et al., 2017) and 1D velocity model (Tab. 1). Seismograms are ground velocities bandpass filtered 1-10 Hz.

For the grid, an estimate of the expected error/uncertainty in the relative arrival time of the S wave can be made. The relative location of the template grid and seismic stations (Fig. 9) together with the velocity model (Tab. 1) defines the maximum difference in the arrival times of the S wave; The S wave originating in the SE top corner of the grid arrives at the KRC station with ∼4.3 s delay compared to SKC station. If the expected uncertainty of the velocity model is 10% (Málek et al., 2005), the expected error in arrival time between the real and synthetic waveforms is up to 0.43 s. This predicted error in arrival time is more pessimistic than the observed 0.22 s in Fig. 2.

2.4 Interpreting focal mechanisms

The similarity of the template waveform to a real event waveform also reflects the similarity in the focal mechanism. Each focal mechanism (FM) without volumetric change can be reconstructed on the basis of five double-couple focal mechanisms (Zahradník and Sokos, 2018, Fig. 3), which implies that an FM of the detected event could be reconstructed from the FM of detecting templates, using similarities as weights. Such can be achieved through a linear combination of moment tensors of the five focal mechanisms, using achieved similarities as weights.

3 Match filter detection routine - Modification for Synthetic Templates

The aim is to detect real events using synthetic templates. Most of the detection routine is similar to the template matching with a real template: select the template seismic event, define the time window relative to P and/or S wave so it covers the waveforms one wants to use for the cross-correlation, run the matching routine to obtain similarity between the template and daily data for each station, sum up the similarity curves, retrieve a time of detected events where the similarity exceeded the detection threshold, and if more detections occur in a defined time window pick the one with highest similarity. Our tests of template matching using Synthetic Templates showed the way the similarity stacking must be modified to account for uncertainties of synthetic arrival times. The ObsPy template matching software (Beyreuther et al., 2010) allows the changes to be implemented; the major required modifications are explained and described below. The resulting scripts for template matching detection with synthetic templates are one of the outputs of this work.

There is a major difference between template matching detection using a real vs. a synthetic template, and it is not in the shape of P or S waveforms. The difference is in the mismatch of relative wave arrival times to some stations because of the inaccuracy in the velocity model. In other words, the real and synthetic P and S wave arrivals overlap at some stations but are time-shifted at others (LBC, POC in Fig. 2). When working in an area without recorded seismicity, the time difference is not known, but it can be estimated from the uncertainty in the 1D velocity model. We estimate the expected error in the relative arrival time to some of the stations t_{err} to ~0.43 s.

Variations in relative arrival times, denoted t_{err}, can lead to misalignment between observed and synthetic waveforms. As a result, a straightforward summation of similarity values across stations may fail to detect an event if arrivals are offset, as illustrated in the central panel of Fig. 4, where no detection is declared. To mitigate this limitation, the method applies a time-smearing approach to similarity traces within a conservative window of $t_{err} = 0.5$ s, slightly broader than the estimated 0.43 s to ensure robustness. This smearing is implemented by computing the local maximum within a sliding window of width t_{err} (i.e., $\pm\frac{1}{2}t_{err}$) using the optimized *move_max* function from the *bottleneck* library (Alon and Yahav, 2021).

The final similarity used for detection is defined as the sum of the smeared similarities divided by n, where n is the required number of components above the cross-correlatio (xc) threshold. If this condition is not met, the final similarity is set to zero. A detection is declared when the final similarity exceeds the xc n threshold. In particular, since detections can involve more than n stations, the resulting final similarity may exceed one. A standard ObsPy parameter, 'minimum time between detections', is also used to prevent repeated detections of the same event. To incorporate similarity smearing into your ObsPy-based pipeline, modify the *similarity_func* used by the correlation

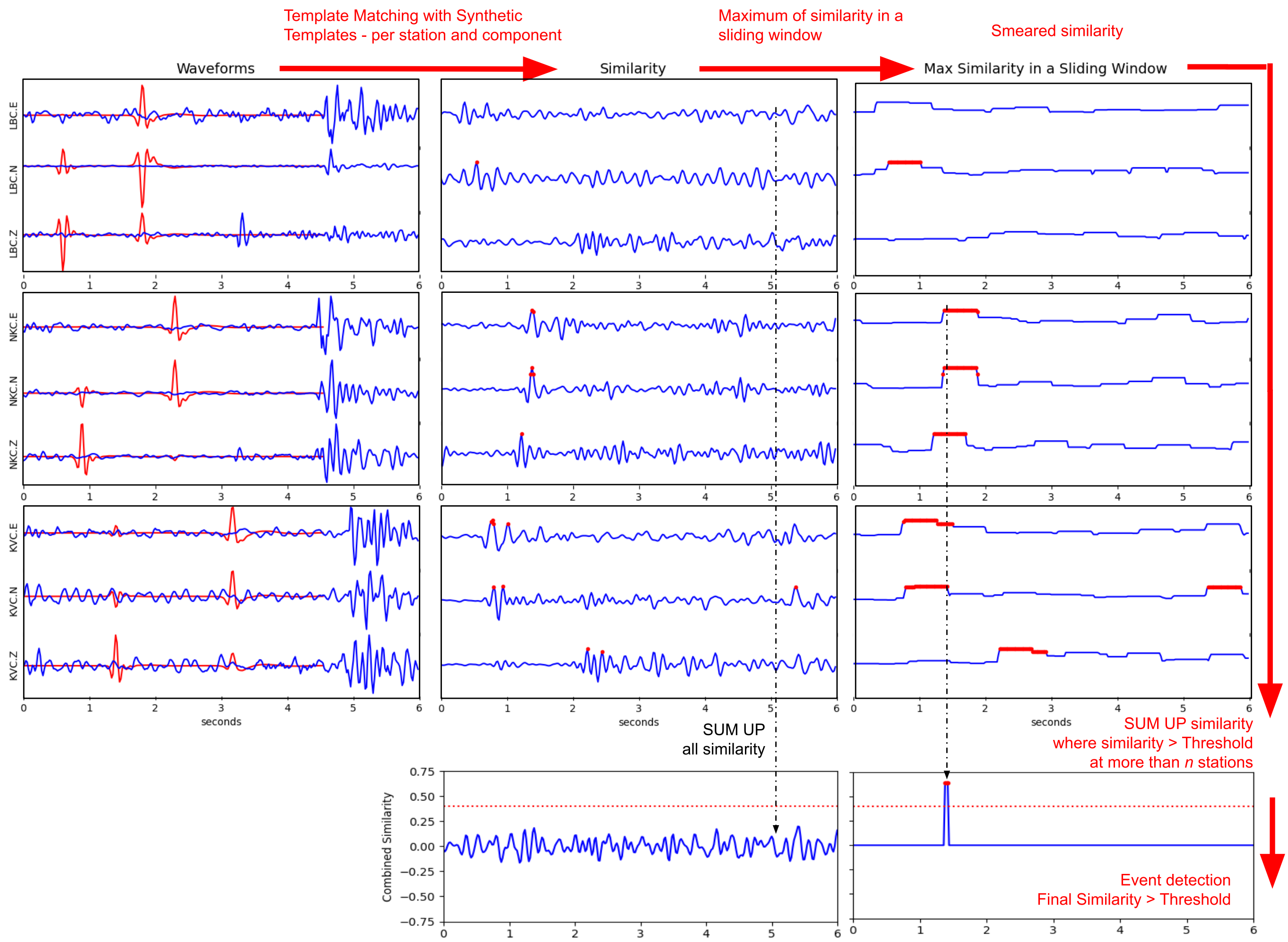

Figure 4 Workflow of Synthetic Template Matching - example of template matching between a real event $M_L 0.63$ 2018/05/18 11:19:38 and a synthetic template with the epicenter 5 km apart. The detection threshold is set to 0.4, the required number of components above the threshold is set to 5 (only for this example on LBC, NKC and KVC station). Left column: Real event waveforms in blue, synthetic template in red. Both filtered 1-10 Hz. Central column: in blue are the similarities (from -1 to 1) - the result of template matching. Similarities above 0.4 are highlighted by red points. The additional diagram at the bottom shows the sum of these similarities divided by 5 - none exceeding the detection threshold 0.4. Right column: Smeared similarities in blue (maximum similarity in a sliding window t_{err} 0.5 s ie. $\pm$0.25 s), values above 0.4 highlighted by red points. Diagram at the bottom shows the final similarities that are created as a sum of smeared similarities divided by 5, but only at time points where at least 5 stations have the smeared similarity above 0.4. This final similarity exceeds the threshold 0.4 only at few time points, but even so the seismic event is detected with similarity 0.64 by this synthetic template located 5 km apart (the synthetic template detecting this event with the greatest similarity 1.3 has the epicenter only 600 m apart from PEPiN location).

worker as shown in Listing 1.

For better understanding of the Synthetic Template Matching workflow, an example detection is shown for three stations (LBC, NKC, and KVC) in Fig. 4. The detection threshold is set to 0.4, the required number of components above the threshold is set to 5. The workflow is presented on the real seismic waveforms of an event (filtered 1-10 Hz, left column in Fig. 4) giving similarities for each component (central column in Fig. 4). The smeared similarities (right column in Fig. 4) are created by the maximum in a sliding window $\pm\frac{1}{2}t_{err}$ (= 0.5 s) and the final similarity in the bottom right corner of Fig. 4 shows a single event detection. Note the importance of the correct estimate of t_{err}, because it influences the span of smeared similarities above the threshold and so the potential of overlap of the smeared similarities above the threshold. In other words, if t_{err} was shorter, there would be no detection in the example in Fig. 4. On the other hand, prolonging t_{err} extends the ability to detect events by a single Synthetic Template.

A Synthetic Template comprises three components (East, North and vertical) for each of the stations and it represents one of the five basic focal mechanisms (Fig. 3) with epicentral location in one of the grid points. When a Synthetic Template detects, the detection is assigned the origin time and magnitude derived from the template (both provided by the ObsPy function) and the exact location and focal mechanism of the template. During Synthetic Template Matching, hundreds of templates can be used for detection, many of which are successful in detecting the same event. The final catalog of detections contains only unique events (within 1 s window) which are assigned the parameters of the template detection with the highest similarity, the number of detecting events and the interpreted focal mechanism (FM).

The focal mechanism assigned to a detected event is interpreted from FM of templates detecting the event and having a hypocenter similar to that of the detecting template with the highest similarity. The resulting FM is a linear combination of FMs converted to moment tensors, weighted by similarity, reduced by the minimal similarity, and converted back to FM.

The software is built to run on many cores in parallel to speed up the process using the *multiprocessing* package of Python (Van Rossum and Drake Jr, 1995).

Listing 1 Implementation of similarity smearing into ObsPy code. The function *similarity_func* requires the parameters to be set directly into it, making the code less transparent.

```
import bottleneck as bn

def similarity_at_subset_stations(ccs, xc_threshold=0.4, nr_components_above_threshold=3,
    sliding_window=0.1):
    """ Calculates mean similarity in a sliding window at 3 (nr_components_above_threshold)
        components with the greatest max(similarity) in the window
    :param ccs: stream - similarity functions for each station and component
    :param xc_threshold: xc threshold both for individual component and final similarity
    :param nr_components_above_threshold: min nr of components required to be above the
        threshold
    :param sliding_window: size of the sliding window in seconds
    :return: Trace with similarity function   """
    window_len_samples = round(sliding_window / ccs.traces[0].stats.delta)
    data_array = np.array([tr.data for tr in ccs]) # converts traces into array
    header = dict(sampling_rate=ccs[0].stats.sampling_rate,
                  starttime=ccs[0].stats.starttime)
    # fast way of calculating max in a sliding window:
    moveMax = bn.move_max(data_array, window_len_samples, axis=1)
    comp_thres = np.sum(moveMax > xc_threshold, axis=0) >= nr_components_above_threshold
    similarity = np.sum(moveMax, axis=0) / nr_components_above_threshold * comp_thres
    return Trace(data=similarity, header=header)

def similarity_func (ccs):
```

```python
    """   Wrapper for the similarity function to set parameters.
   :param ccs (dict): Similarity values for each station and component.
   :return: Resulting similarity score.   """
     return similarity_at_subset_stations(ccs, xc_threshold=0.4, nr_components_above_threshold
         =9, sliding_window=0.5)

def correlation_worker(args):
    """  Worker function for processing a chunk of the stream or template.  """
    stream_chunk, template, height, distance, template_names, template_magnitudes,
        similarity_func = args
    return correlation_detector(stream_chunk, template, height,  distance, template_names=
        template_names, template_magnitudes=template_magnitudes, plot=None, similarity_func=
        similarity_func  )
```

4 Results

The results of Synthetic Template Matching are presented with two detection thresholds: the higher cross-correlation threshold ($xc\,0.4$) that ensures zero false detection, and the lower ($xc\,0.35$) improving the magnitude of completeness from M_C-0.1 to M_C-0.3 (red points for $xc\,0.4$ and orange points for $xc\,0.35$ in Fig. 5a).

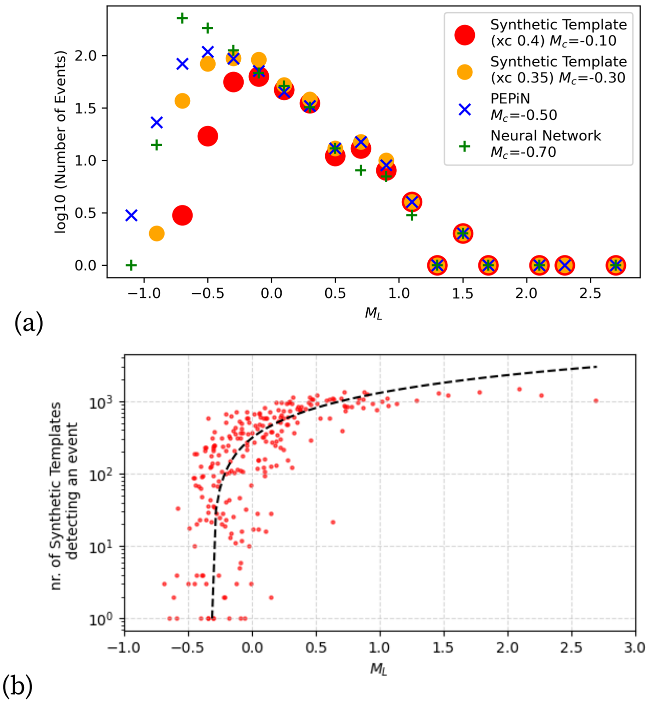

Figure 5 (a) Gutenberg Richter distribution of seismic catalogs by Synthetic Template Matching (red points $xc\,0.4$, orange points $xc\,0.35$), PEPiN (blue crosses) and Neural Network (green crosses) with interpreted magnitudes of completeness M_C. Magnitude of completeness M_C is determined using the maximum curvature method (Pavlenko and Zavyalov, 2022). Magnitude is derived by PEPiN or extrapolated from it. (b) Number of Synthetic Templates detecting an event vs. event's M_L (Detecting with $xc\,0.4$). Red points represent events detected by both Synthetic Template Matching and PEPiN. Black dashed line is linear interpolation of the red points; it curves due to logarithmic display of the y axis.

For testing Synthetic Template Matching technique, we chose daily seismograms from the period 2008 - 2018 for which focal mechanisms were available (Vavryčuk et al., 2022). The test day is chosen to be 18^{th} May 2018 (Julian day 2018.138), with a focal mechanism available for 7 events $1.2 < M_L < 3.1$ (Vavryčuk et al., 2022): 3 located in the Southern cluster slightly outside the test network of eight stations (see the minor activity in South cluster NW of station MAC in Fig. 1), and 4 in the North seismic cluster North of the NKC station and East of LBC station; see the major activity in Fig. 1. The depth of these events is 8.2 - 10 km.

There are 507 seismic events detected by PEPiN ($-0.55 < M_L < 2.7$) on 18th May 2018, automatically located mainly in the North cluster, few in the Southern cluster. The magnitude of completeness of PEPIN is M_C-0.5 (blue crosses in Fig. 5a).

The Artificial Neural Network (ANN) detects 724 events on 18th May 2018. Since the ANN does not provide location or magnitude, the magnitude of completeness is determined when the ANN catalog is matched to PEPiN's and the magnitudes are extrapolated for unmatched events based on maximum recorded amplitude, with the awareness that an exceptionally high magnitude can be result of a noise spike. Consequently, the magnitude of completeness is determined M_C-0.7 (green crosses in Fig. 5a). The ANN catalog is not compared to catalogs by PEPiN and Synthetic Template Matching on one-to-one match because several of the ANN event-detection comprises of multiple events.

The results of the Synthetic Template Matching are examined in greater detail in the following subsections. Specifically, we explore:

1. How many templates are typically associated with the detection of a single event?

2. How does the performance of the Synthetic Template Matching compare to that of the PEPiN approach, particularly in terms of missed and false detections for events with $M_L > 0$?

3. How do the event locations compare?

4. Furthermore, we assess whether the Synthetic Template Matching can provide insight into focal mechanisms, and how these inferred mechanisms align with those presented by Vavryčuk et al. (2022).

4.1 Single event detected by grid of Synthetic Templates

How a single event detection looks like when a network of Synthetic Templates is used for detection? To examine the effect, we select an event $M_L 1.8$ from the central cluster (depth 10 km) that occurred at 3:23:10.96 at night on 18th May 2018, with focal mechanism strike 348°, dip 87°, rake 31° (respectively 256°, 59°, 176°; Vavryčuk et al., 2022).

This event was detected by 1353 Synthetic Templates (similarity 0.68-1.37, origin time assigned 3:23:11.67 - 3:23:14.2), being one of the most pronounced seismic events on 18th May 2018, see Fig. 5b. The template that showed the greatest similarity is located horizontally 1.3 km from the location associated with the focal mechanism (Vavryčuk et al., 2022), 924 m from manual location by IG CAS (Institute of Geophysics, 2024), and 477 m from PEPiN location. All four are lined on the NNE line, see stars in Fig. 6a. The depth by Synthetic Template Matching is 8 km being 1.6 - 2.0 km shallower than the other locations (stars in Fig. 6b). The uncertainty in depth by Synthetic Template Matching is great, since all 25 templates of the particular horizontal coordinates detect this event with high similarity (1.06 - 1.37); it implies that the focal mechanism has limited effect on the similarity and so on the detection.

4.2 Synthetic Templates Matching results

We compare the performance of the Synthetic Template Matching using two detection thresholds, $xc\,0.4$ and $xc\,0.35$

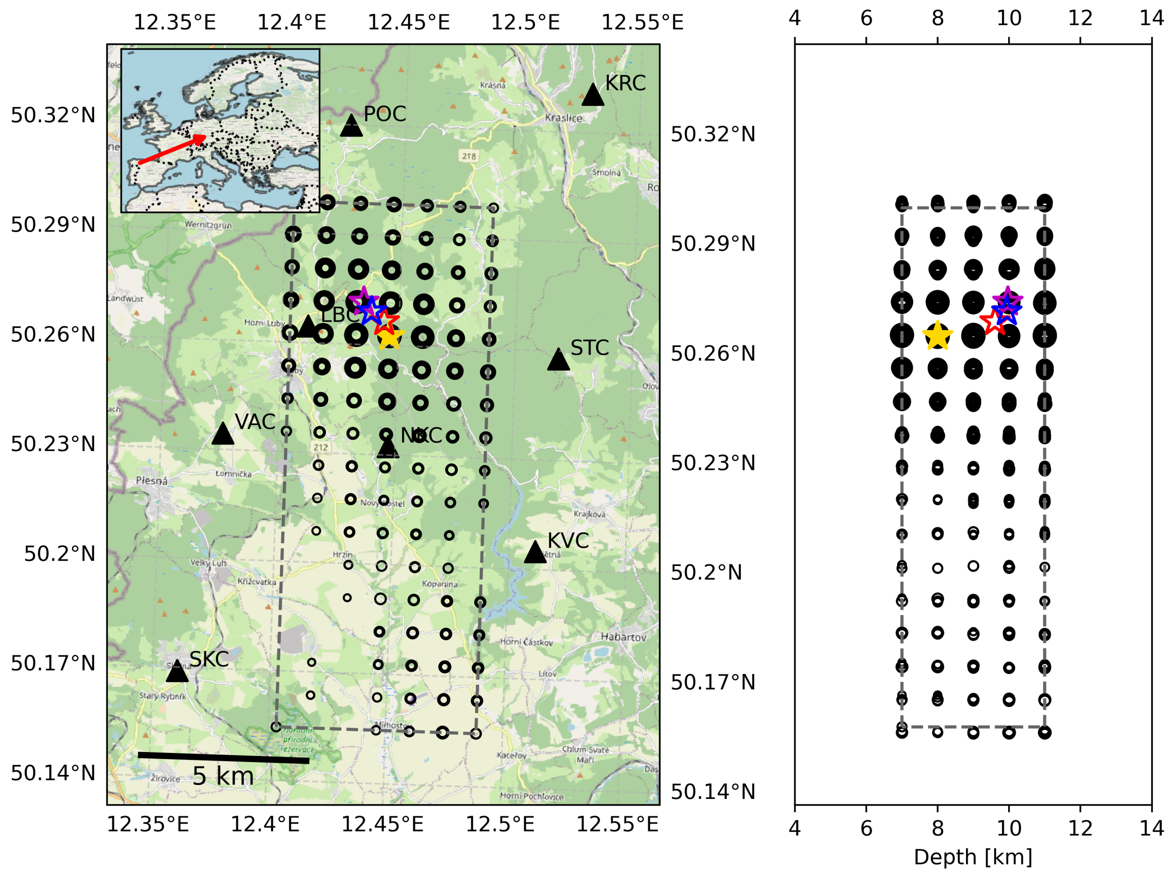

(a) (b)

Figure 6 Single event detection by multiple Synthetic Templates. Event $M_L 1.8$ 3:23:10.96 18th May 2018. (a) Map view of West Bohemia region, zoom of Fig. 1. Black rings - locations of templates detecting the event, rings's size reflect similarity between template and the event. Yellow filled star - template with greatest similarity = assigned event location. Red star - PEPiN location. Magenta star - location from focal mechanism catalog (Vavryčuk et al., 2022). Blue star - manual location by IG CAS (Institute of Geophysics, 2024). (b) Projection of all the locations to North-South plane, depth cross-section. Symbols similar to (a).

The initial output of Synthetic Template Matching is a detection catalog which comprises all detections by all the templates. This initial catalog is later converted to a catalog of unique seismic events: The location, magnitude, and detection time of the template with the highest similarity is assigned to each event detection. An event's focal mechanism is based on the focal mechanism of all the templates with the final location (more details are given in the following section: Focal Mechanism effect on detection). The magnitude of an event assigned by the cross-correlation technique is converted to M_L by PEPiN (see the following paragraph). Each event is also assigned the number of templates that detected it. Events in the Synthetic Template Matching catalog are than associated to events in the PEPiN's catalog based on similarity of origin times.

As the Q-factors are only rough estimates (Tab. 1), the synthetic waveforms do not provide realistic amplitudes in terms of the absolute values in m/s. Consequently, also the magnitude (M_w) determined by the cross-correlation detector is misled and the conversion to M_L by Káldy and Fischer (2025, $M_L = 1.41 * M_w - 0.78$, Eq. 4, green line in supplement Fig. ML_vs_MW) had to be replaced by $M_L = 0.790 * M_w(SyntTempl) - 2.204$ (black line in supplement Fig. ML_vs_MW). This relation comes from comparing M_L and $M_w(SyntTempl)$ of events detected both by PEPIN and by Synthetic Template Matching with xc threshold 0.4 (red points in the supplement Fig. ML_vs_MW).

4.2.1 Detection with xc threshold 0.4

Detection by 2 975 Synthetic Templates (varying in location and focal mechanism) resulted in 97 400 detections when the xc threshold is set to 0.4 and the minimum time between detections is 3 s. Many of individual events were detected by hundreds of templates (up to 1 495 templates), and only 17 were located by a single template (Fig. 5b). Consequently, these nearly 100 thousands detections resulted in the detection of 264 unique seismic events: 244 of them were matched with PEPiN detections, 20 were detected only by Synthetic Template Matching. The time - magnitude distribution of detection both by the Synthetic Template Matching and PEPiN is shown in Fig. 7a; the events detected by Synthetic Template Matching (in red points and black stars) envelope the activity detected only by PEPiN (in blue) with several exceptions. The magnitude of completeness M_C -0.1 is less favorable by $M_L 0.4$ than M_C -0.5 by PEPiN (Fig. 5a).

(a) XC threshold 0.4:

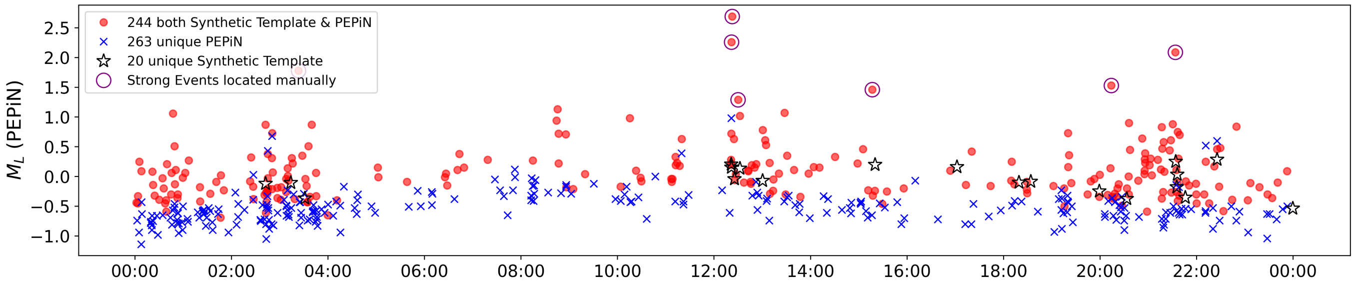

(b) XC threshold 0.35:

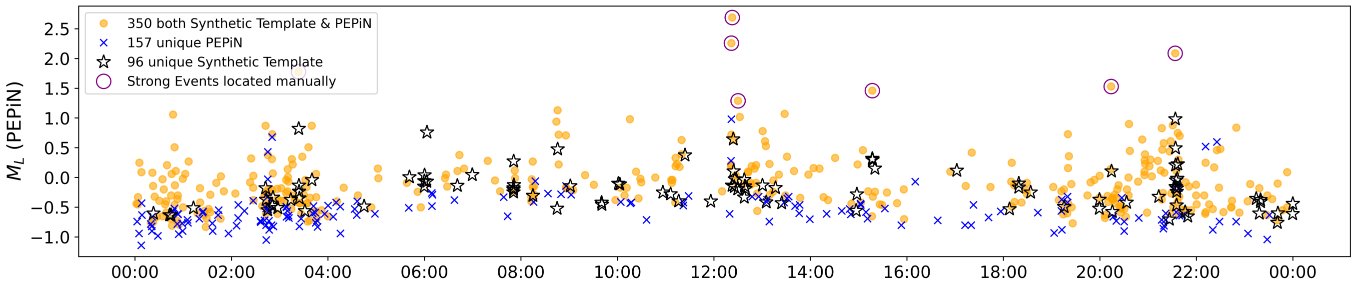

Figure 7 Detection performance: Synthetic Template Matching vs PEPiN, different xc threshold. (a) XC threshold 0.4: 19 detected only by Synthetic Template Matching (black stars), 244 events detected by both Synthetic Template Matching and PEPiN (red points). 263 events detect uniquely by PEPiN (blue crosses). (b) XC threshold 0.35: 96 detected only by Synthetic Template Matching (black stars, 56 are real local events), 351 events detected by both Synthetic Template Matching and PEPiN (orange points). 157 events detected uniquely by PEPiN (blue crosses). Purple circles refer to the seven strong events with manual locations and focal mechanisms.

The Synthetic Template Matching missed 15 events $M_L \geq M_C$ -0.1, 9 events $M_L \geq 0.0$ (only 4 of them were located by PEPiN within the network). On the other hand, the Synthetic Template Matching provided 20 seismic events in addition to PEPiN detection (14 $M_L \geq M_C(-0.1)$, 8 events $M_L \geq 0.0$); all visually examined and recognized real without a doubt. See Fig. 8 for an example event detected by both PEPiN and the Synthetic Template Matching (a), an event detected only by PEPiN (b), and an event detected only by Synthetic Template Matching (c).

More than 85% (227 of 264) of events were detected with 10 or more Synthetic Templates (Fig. 5b), which implies that the number of templates could be reduced without affecting the detection ability noticeably, leaving out mostly $M_L < 0$ events.

With the detection threshold 0.4 the detection by Synthetic Template Matching does not outperform the automated detection by amplitude-based PEPiN, but it does not create a single false detection.

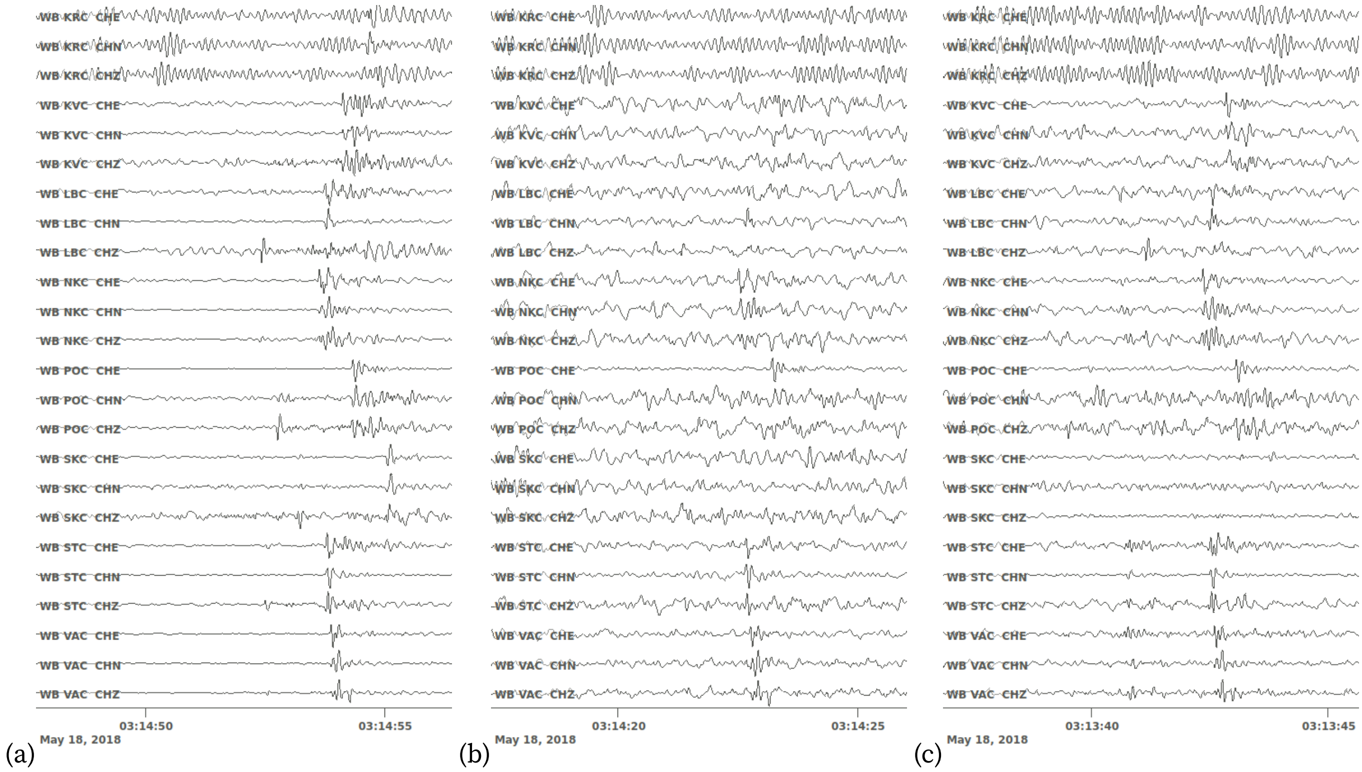

Figure 8 Example of detected seismic events. (a) $M_L 0.3$ detected both by PEPiN & Synthetic Template Matching (b) $M_L{-}0.5$ detected only by PEPiN (c) $M_L{-}0.3$ detected only by Synthetic Template Matching. All band-pass filtered 1-10 Hz, displayed by Snuffler (Pyrocko).

4.2.2 Detection with xc threshold 0.35

The time - magnitude distribution of detection both by the Synthetic Template Matching with $xc\ 0.35$ and PEPiN is shown in Fig. 7b; the events detected by Synthetic Template Matching (in orange points and black stars) envelope and overlap the activity detected only by PEPiN (in blue). The magnitude of completeness $M_C{-}0.3$ is less favorable by $M_L 0.2$ than $M_C{-}0.5$ by PEPiN, but it improved the detection with $xc\ 0.4$ by $M_L 0.2$ (Fig. 5a).

The template matching on the grid of Synthetic Templates with the detection threshold decreased to 0.35 created more than twice detections (223 364) than with $xc\ 0.4$, resulting in 446 unique seismic events (1.8 times more than with $xc\ 0.4$, similarities 0.63 - 1.48). As such, it performs closer to PEPiN , sharing 350 detections and missing 157 PEPiN detections (5 of 6 with $M_L > 0$ are located outside the network).

There are 96 unique events detected by Synthetic Template Matching, with $-0.14 < M_L < 0.98$ (similarity 0.63 - 1.2). The visual examination of these unique events by Synthetic Template Matching shows that half of them (49) are real local events, 11 distant or low-frequency (LFE) events, and 36 noise or highly uncertain detections. The high M_L of these unique events does not ensure that they are real or local (two events with $M_L > 0.7$ are noise, one is a distant seismic event), but due to Synthetic Template Matching there are 9 extra real local events with $0 < M_L < 0.7$ (of 16 proclaimed ones) that were not detected by PEPiN. That is not improvement to $xc\ 0.4$ which detected 8 additional events with $M_L < 0$.

Although detection with Synthetic Template Matching with the xc threshold 0.35 provides a more complete catalog, it also generates false detections, some of them of relatively high interpreted magnitude ($0.7 < M_L < 1$).

4.3 Location by Synthetic Template Matching

The location of each detected event is assigned based on the template that yielded the highest similarity score. Given that the template grid spacing is 1 km, this imposes a minimum horizontal location uncertainty of $\pm\frac{1}{\sqrt{2}}$ km. An example of a multi-template detection for a single event (Fig. 6) indicates that, for high-magnitude events, the epicentral location uncertainty lies within this expected range when compared to manual and PEPiN-derived locations. In contrast, the same comparison highlights that the depth estimates are subject to considerably greater uncertainty.

When epicentral locations are compared for all the 244 mutual events detected by PEPin and Synthetic Template Matching ($xc\ 0.4$, Fig. 9a) the average epicentral difference is 1.2 km (median 1.0 km, 90$^{\text{th}}$ percentile 2.1 km and max 8.0 km). The depths interpreted by Synthetic Template Matching are slightly deeper, with the average absolute difference being 1.4 km (median 1.3 km, 90$^{\text{th}}$ percentile 2.3 km and max 8.0 km, differences pointed by gray lines in Fig. 9b).

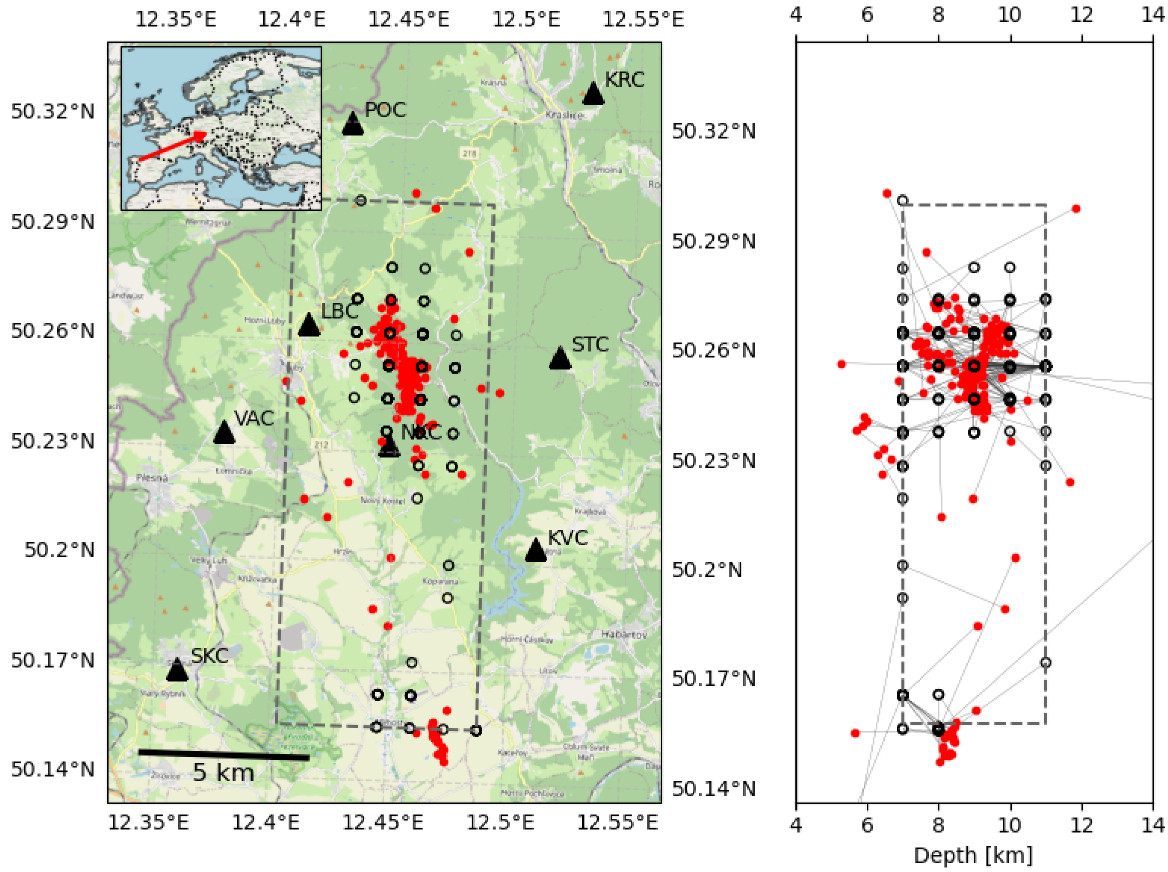

(a) (b)

Figure 9 Locations by Synthetic Template Matching vs. by PEPiN (xc threshold 0.4). (a) Map view of West Bohemia region with seismic stations used in this study. Red points - events detected by Synthetic Template Matching - locations by PEPiN. Black rings - events detected by Synthetic Template Matching - locations from detecting templates. For other details see Fig. 6. (b) Projection of all the locations to North-South plane, depth cross-section. Comparison of locations by PEPiN and Synthetic Template Matching: Light gray lines connect the two locations of a single event detection. Symbols similar to (a).

The locations were also compared for the 7 strong seismic events with manual locations $1.3 < M_L < 2.7$ (purple circles in Fig. 7). The epicentral location varies in average 0.5 km (0.3 - 0.8 km) from PEPiN, and 1.2 km (1.0 - 1.5 km) from location used for focal mechanisms (Vavryčuk et al., 2022) when the event is located in the Northern cluster (center of the network). The difference in epicenter is 2.8 km (1.2 - 5.9 km) vs. 1.7 km (all 1.7 km) when located in the

Southern cluster, outside the seismic network, and at the edge of the template grid. With an exception of a single PEPiN location, the epicentral location by Synthetic Template Matching is closer to PEPiN, which uses a similar set of seismic stations, than to location for FM, which uses 22 - 23 stations. The depths interpreted by Synthetic Template Matching are shallower (with a single exception) in average 1.2 km compared to PEPiN and 1.5 km compared to FM locations.

In conclusion, the Synthetic Template Matching method demonstrates robust horizontal localization, the accuracy is inherently limited by the template grid resolution, but depth estimations remain less constrained.

4.4 Focal Mechanism effect on detection

To check what is the effect of template's focal mechanism (FM) on detection, we show in Fig. 10a the contribution of different FM to event detection. It turns out that this effect is limited: if only a single FM was chosen for all grid points, it would detect an average of 220 (194 - 234) events instead of 264 events when all templates are used. Interestingly, the FM with the highest detection rate (pure strike-slip: strike 0°, dip 90° and rake 0°) is similar to FM of four strong events in the North cluster (Vavryčuk et al., 2022, strike-slip: strike 348°, dip 87°, rake 31°).

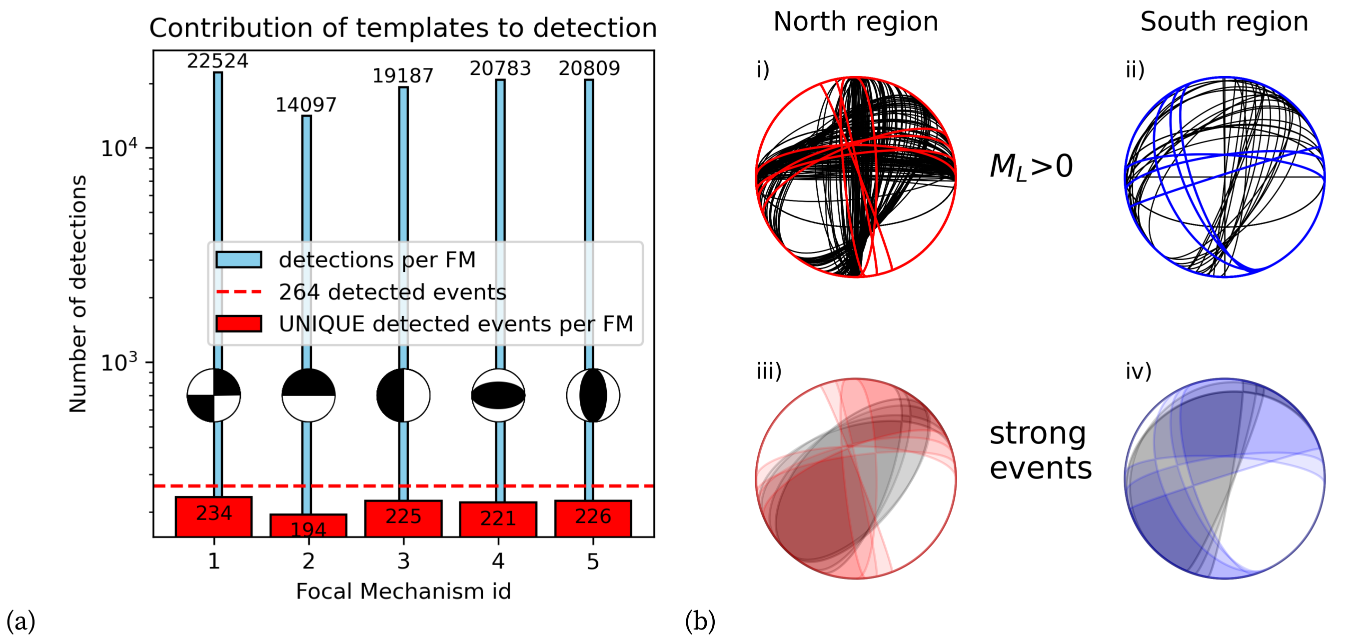

Figure 10 (a) Contribution of templates according to focal mechanisms (FM): total number of detections in light blue and unique events in red. The red dashed line points the number of unique events that are detected using all templates with all focal mechanisms ($xc\,0.4$). (b) Focal mechanisms interpreted by Synthetic Template Matching in black vs. focal mechanism manually determined for 7 strongest events of the day by Vavryčuk et al. (2022) in color. Events from the center of the seismic network - the North Region - in i) and iii), manual FM in red. Events from outside the seismic network - the South region - in ii) and iv), manual FM in blue.

In Fig.10b(i), the focal mechanisms (FMs) interpreted via Synthetic Template Matching for events with $M_L > 0$ are plotted atop each other and compared to those reported by Vavryčuk et al. (2022), all originating from the Northern cluster. The Synthetic Template Matching solutions (shown in black) reveal two distinct patterns: the first group of FMs closely matches the strike-slip mechanisms published by Vavryčuk et al. (2022) (in red), while the second group corresponds to reverse faulting, exemplified by a representative solution with strike 253°, dip 43°, and rake 134°. Notably, one of the fault planes of the reverse solutions is nearly aligned with the nodal plane of the aforementioned strike-slip events. This reverse-faulting pattern is also observed for the four strongest events within the Northern region, as indicated by the black mechanisms in Fig.10b(iii). In contrast, the Southern seismic cluster exhibits predominantly reverse to low-angle reverse faulting mechanisms (Fig. 10b(ii,iv), which show limited agreement with the cataloged FMs by Vavryčuk et al. (2022).

Interestingly, when the number of detected events in Fig. 10a is used as weights for estimating the overall FM, the interpreted FM is reverse fault (strike 242°, dip 39°, rake 121°) similar to the interpreted FM of strong events (strike 253°, dip 43°, rake 134°, one of black FMs in Fig. 10b(iii)).

Although the initial observations of FM's effect on detection did not imply the interpretability of FM , FM could be interpreted consistently and in alignment with FM by Vavryčuk et al. (2022) for events located in the Northern cluster, i.e. inside of the seismic network. The interpretation of FM of the Southern cluster, located outside the network, was also quite consistent, but did not align with FM by Vavryčuk et al. (2022) and should be interpreted with care.

5 Summary and discussion

The study aims to test the performance of synthetic seismograms as templates for template matching detection using cross-correlation, and to compare it with two algorithms routinely detecting seismicity in West Bohemia: First, the automated seismic detector and locator PEPiN (Fischer, 2003; Káldy and Fischer, 2025). Second, the Artificial Neural Network (ANN) detection (Doubravová and Horálek, 2019). Last, Synthetic Template Matching was found capable of estimating the focal mechanism, which is compared to the focal mechanism by Vavryčuk et al. (2022).

Synthetic Template Matching utilizes a grid of templates that vary in hypocenter locations and focal mechanisms. The locations are to cover the area of interest; the focal mechanisms are the five elementary focal mechanisms (FM) (Zahradník and Sokos, 2018), which are independent of the FM expected in the region. The resulting catalog of events detected by Synthetic Template Matching comprises the origin time, similarity, M_w (later converted to M_L), and location (longitude, latitude, and depth) taken from the template of highest similarity; in the catalog there is also the number of templates detecting the event and focal mechanism interpreted from detecting templates of similar hypocenter.

In the WEBNET test scenario where the epicentral distance and depth are up to 10 km (seismograms band-pass filtered 1-10 Hz) and the Synthetic Templates created with the 1D velocity model, the Synthetic Template Matching detected 264, resp. 446 seismic events with the xc threshold 0.4 resp. 0.35 (Fig. 7a, resp. b); the magnitude of completeness being $M_C{-}0.1$, resp. $M_C{-}0.3$ (red, resp. orange points in Fig. 5). In the $xc\,0.4$ scenario are all the detected events real and local, but in the $xc\,0.35$ case, there are many false detections, two even with magnitudes $M_L > 0.7$, and some detected events are distant or low-frequency ones (LFE).

Although Synthetic Template Matching detects hundreds of events per day, confidently with magnitude below zero, it does not outperform the automated detector and locator PEPiN or Neural Network in terms of M_C (Fig. 5). Another study on detection using synthetic seismograms as templates is done by Chamberlain and Townend (2018). It claimed that synthetic templates can serve for the detection of several real earthquakes on the local scale, outperforming energy detectors in swarm detection and detecting 29 of 41 events detected with real templates ($T_S - T_P \sim 0.7\ s$). In contrast on the regional scale, in the aftershock sequence of the $M6.0$ Wanaka earthquake ($T_S - T_P \sim 5\ s$), the synthetic template served to detect 248 events compared to 1 678 and 682 events by the real template and sta/lta method. The synthetic templates in Chamberlain and Townend (2018) mimicked the real templates in terms of location and focal mechanism; this is not the case in this study, which is probably the reason for the lower performance on the local scale.

The location assigned to an event detected by Synthetic Template Matching is limited to the grid points, spaced by 1 km. Compared to locations by other methods, the epicenters vary in average by 1.2 km from PEPiN's locations, and 0.5 km from manual location of strong events (Vavryčuk et al., 2022). This applies when within the network, twice more when outside. The assigned depths should be interpreted with caution, although they vary from others only by 1.5 km. If the need for a more precise location arises, interpolation between grid points based on similarity is possible.

The interpretation of focal mechanisms (FMs) using Synthetic Template Matching on eight WEBNET stations reveals a consistent and mostly geologically plausible pattern for events inside the network; two dominant FM types emerged: one closely matching the strike-slip mechanisms reported by Vavryčuk et al. (2022), and another corresponding to reverse faulting with nodal planes adjacent to those of the strike-slip solutions. These FM's are different in geological interpretation, but much alike in terms of polarity and amplitude variations.

The Python codes performing Synthetic Template Matching are based on packages ObsPy (Beyreuther et al., 2010) and Pyrocko (Heimann et al., 2017, 2020, 2019) and processing one day's worth of data from eight seismic stations with 2 975 Synthetic Templates requires around five hours on a system with 4 CPU cores. The code for Synthetic Template Matching is made available, together with the daily seismograms, Synthetic Templates, and the input and resulting catalogs for the test day.

In conclusion, although Synthetic Template Matching is outperformed by PEPiN and Artificial Neural Network in terms of the magnitude of completeness (M_C difference 0.2 - 0.6), it delivers great value in deriving focal mechanisms and in relatively precise epicentral locations.

Acknowledgements

The article was created with support of the project "SYNERGYS - systems for energy synergies" (co-funded by the EU Operational programme Just Transition) No. $CZ.10.02.01/00/22\_002/0000172$.

The map in Fig. 1, Fig. 6a and Fig. 9a was created using PYGMT.

We thank the anonymous reviewers for their valuable comments and constructive suggestions, which helped to improve the quality of this article.

Data and code availability

The Python codes for Synthetic Template Matching are made available, together with the daily seismograms, Synthetic Templates (also Pyrocko code for creation), and the input and resulting catalogs for the test day. The same location contains supplement Figure `ML_vs_MW.png`. All are available at (Google disk now, but will be transferred to Zenodo when approved by reviewers):

https://drive.google.com/drive/folders/1cE5Rw6xbxThnUpovNqxcchOdGKirdpfC?usp=sharing

(or by email to the corresponding author).

Competing interests

The authors have no competing interests.

References

Alon, U. and Yahav, E. GNN Bottleneck: On the Bottleneck of Graph Neural Networks and its Practical Implications. https://github.com/tech-srl/bottleneck, 2021. Accessed: 2025-05-21, presented in https://openreview.net/forum?id=i80OPhOCVH2.

Beyreuther, M., Barsch, R., Krischer, L., Megies, T., Behr, Y., and Wassermann, J. ObsPy: A Python Toolbox for Seismology. *Seismological Research Letters*, 81(3):530–533, 05 2010. doi: 10.1785/gssrl.81.3.530.

Chamberlain, C. J. and Townend, J. Detecting Real Earthquakes Using Artificial Earthquakes: On the Use of Synthetic Waveforms in Matched-Filter Earthquake Detection. *Geophysical Research Letters*, 45(21):11,641–11,649, 2018. doi: 10.1029/2018GL079872.

Chamberlain, C. J., Boese, C. M., and Townend, J. Cross-correlation-based detection and characterisation of microseismicity adjacent to the locked, late-interseismic Alpine Fault, South Westland, New Zealand. *Earth and Planetary Science Letters*, 457:63–72, 2017. doi: 10.1016/j.epsl.2016.09.061.

Clarke, H., Eisner, L., Styles, P., and Turner, P. Felt seismicity associated with shale gas hydraulic fracturing: The first documented example in Europe. *Geophysical Research Letters*, 41(23):8308–8314, 2014. doi: 10.1002/2014GL062047.

Diaferia, G., Valoroso, L., Improta, L., and Piccinini, D. A High-Resolution Seismic Catalog for the Southern Apennines (Italy) Built Through Template-Matching. *Geochemistry, Geophysics, Geosystems*, 25(3):e2023GC011160, 2024. doi: 10.1029/2023GC011160.

Doubravová, J. and Horálek, J. Single Layer Recurrent Neural Network for detection of local swarm-like earthquakes—the application. *Geophysical Journal International*, 219(1):672–689, 07 2019. doi: 10.1093/gji/ggz321.

Essing, D. and Poli, P. Spatiotemporal Evolution of the Seismicity in the Alto Tiberina Fault System Revealed by a High-Resolution Template Matching Catalog. *Journal of Geophysical Research: Solid Earth*, 127(10):e2022JB024845, 2022. doi: 10.1029/2022JB024845.

Fallahi, M. J., Mousavi, S., Korn, M., Sens-Schönfelder, C., Bauer, K., and Rößler, D. 3D velocity structure of upper crust beneath NW Bohemia/Vogtland. In *Geophysical Research Abstracts*, volume 15, pages EGU2013–8678. EGU General Assembly 2013, 2013.

Fischer, T. The August–December 2000 earthquake swarm in NW Bohemia: the first results based on automatic processing of seismograms. *Journal of Geodynamics*, 35(1):59–81, 2003. doi: 10.1016/S0264-3707(02)00054-6.

Gibbons, S. J. and Ringdal, F. The detection of low magnitude seismic events using array-based waveform correlation. *Geophysical Journal International*, 165(1):149–166, 04 2006. doi: 10.1111/j.1365-246X.2006.02865.x.

Grigoli, F., Cesca, S., Rinaldi, A. P., Manconi, A., López-Comino, J. A., Clinton, J. F., Westaway, R., Cauzzi, C., Dahm, T., and Wiemer, S. The November 2017 M_w 5.5 Pohang earthquake: A possible case of induced seismicity in South Korea. *Science*, 360(6392):1003–1006, 2018. doi: 10.1126/science.aat2010.

Güralp Systems Limited. *Güralp 3ESP Compact, Operator's Guide*. Midas House, Calleva Park, Aldermaston READING, RG7 8EA. England, issue e edition, September 2021. file:///home/eva/Downloads/MAN-C3E-0001.pdf. Document No: MAN-C3E-0001.

Hanks, T. C. and Kanamori, H. A moment magnitude scale. *Journal of Geophysical Research: Solid Earth*, 84(B5):2348–2350, 1979. doi: 10.1029/JB084iB05p02348.

Harris, D. B. A waveform correlation method for identifying quarry explosions. *Bulletin of the Seismological Society of America*, 81(6): 2395–2418, 12 1991. doi: 10.1785/BSSA0810062395.

Heimann, S., Kriegerowski, M., Isken, M. P., Cesca, S., Daout, S., Grigoli, F., Juretzek, C., Megies, T., Nooshiri, N., Steinberg, A., Sudhaus, H., Vasyura-Bathke, H., Willey, T., and Dahm, T. Pyrocko - An open-source seismology toolbox and library. *Potsdam : GFZ Data Services*, 2017. doi: 10.5880/GFZ.2.1.2017.001.

Heimann, S., Vasyura-Bathke, H., Sudhaus, H., Isken, M. P., Kriegerowski, M., Steinberg, A., and Dahm, T. A Python framework for efficient use of pre-computed Green's functions in seismological and other physical forward and inverse source problems. *Solid Earth*, 10(6): 1921–1935, 2019. doi: 10.5194/se-10-1921-2019.

Heimann, S., Kriegerowski, M., Isken, M., Vasyura-Bathke, H., Cesca, S., Nooshiri, N., Petersen, G., Metz, M., Steinberg, A., Sudhaus, H., , and Dahm, T. Pyrocko - A Versatile Software Framework for Seismology. *EGU General Assembly 2020, Online*, pages EGU2020–18734, 2020. doi: 10.5194/egusphere-egu2020-18734, 2020.

Institute of Geophysics. West Bohemia Local Seismic Network [Data set], 1991. 10.7914/SN/WB. doi: 10.7914/SN/WB.

Institute of Geophysics. WEBNET Seismic Network: Earthquake Catalogs, 2024. https://www.ig.cas.cz/vyzkum-a-vyuka/observatore/lokalni-seismicka-sit-webnet/katalogy-webnet/. Accessed: 2025-05-21.

Janská, E. and Eisner, L. Ongoing seismicity in the Dallas-Fort Worth area. *The Leading Edge*, 31(12):1462–1468, 2012. doi: 10.1190/tle31121462.1.

Karousová, H., Plomerova, J., and Babuska, V. Three-dimensional velocity model of the crust of the Bohemian Massif and its effects on seismic tomography of the upper mantle. *Studia Geophysica et Geodaetica*, 56, 01 2012. doi: 10.1007/s11200-010-0065-z.

Káldy, E. and Fischer, T. Microseismic network sensitivity in case of no seismic activity. *Journal of Seismology*, 27(4):627–641, 2023. doi: 10.1007/s10950-023-10134-y.

Káldy, E. and Fischer, T. Performance of Automatic Detector &; Locator Tested on Synthetic Seismograms: Case Study from Litoměřice in Czech Republic. *Seismica*, 4(1), Apr. 2025. doi: 10.26443/seismica.v4i1.1373.

Levin, B., Sasorova, E., Borisov, S., and Borisov, A. Estimating the parameters of small earthquakes and their signals. *Journal of Volcanology and Seismology*, 4(3):203–212, 2010. doi: 10.1134/S074204631003005X.

Mousavi, S., Bauer, K., Korn, M., and Hejrani, B. Seismic tomography reveals a mid-crustal intrusive body, fluid pathways and their relation to the earthquake swarms in West Bohemia/Vogtland. *Geophysical Journal International*, 203(2):1113–1127, 10 2015. doi: 10.1093/gji/ggv338.

Málek, J., Horálek, J., and Janský, J. One-Dimensional qP-Wave Velocity Model of the Upper Crust for the West Bohemia/Vogtland Earthquake Swarm Region. *Studia Geophysica et Geodaetica*, 49(4):501–524, 2005. doi: 10.1007/s11200-005-0024-2.

Novotný, O. A preliminary seismic model for the region of the West-Bohemian earthquake swarms. *Studia Geophysica et Geodaetica*, 40: 353–366, 1996.

Pavlenko, V. and Zavyalov, A. Comparative Analysis of the Methods for Estimating the Magnitude of Completeness of Earthquake Catalogs. *Izvestiya, Physics of the Solid Earth*, 58, 2022. doi: 10.1134/S1069351322010062.

Rodgers, A., Harris, D., and Pasyanos, M. A model-based signal processing approach to seismic monitoring. *Proceedings of 28th Seismic Research Review: Ground-Based Nuclear Explosion Monitoring Technologies*, pages 455–464, 2006.

Ross, Z. E., Trugman, D. T., Hauksson, E., and Shearer, P. M. Searching for hidden earthquakes in Southern California. *Science*, 364(6442): 767–771, 2019. doi: 10.1126/science.aaw6888.

Shearer, P. M. *Introduction to Seismology*. Cambridge University Press, 2009.

Shelly, D. R., Beroza, G. C., Ide, S., and Nakamula, S. Low-frequency earthquakes in Shikoku, Japan, and their relationship to episodic tremor and slip. *Nature*, 442:188–191, 2006. doi: 10.1038/nature04931.

Shelly, D. R., Hill, D. P., Massin, F., Farrell, J., Smith, R. B., and Taira, T. A fluid-driven earthquake swarm on the margin of the Yellowstone caldera. *Journal of Geophysical Research: Solid Earth*, 118(9):4872–4886, 2013. doi: 10.1002/jgrb.50362.

Shelly, D. R., Ellsworth, W. L., and Hill, D. P. Fluid-faulting evolution in high definition: Connecting fault structure and frequency-magnitude variations during the 2014 Long Valley Caldera, California, earthquake swarm. *Journal of Geophysical Research: Solid Earth*, 121(3): 1776–1795, 2016. doi: 10.1002/2015JB012719.

Van Rossum, G. and Drake Jr, F. L. *Python tutorial*. Centrum voor Wiskunde en Informatica Amsterdam, The Netherlands, 1995.

Vavryčuk, V., Adamová, P., Doubravová, J., and Horálek, J. Moment tensor catalogue of earthquakes in West Bohemia from 2008 to 2018. *Earth System Science Data*, 14(5):2179–2194, 2022. doi: 10.5194/essd-14-2179-2022.

Wang, R. A simple orthonormalization method for stable and efficient computation of Green's functions. *Bulletin of the Seismological Society of America*, 89(3):733–741, 06 1999. doi: 10.1785/BSSA0890030733.

Wang, R., Heimann, S., Zhang, Y., Wang, H., and Dahm, T. Complete synthetic seismograms based on a spherical self-gravitating Earth model with an atmosphere–ocean–mantle–core structure. *Geophysical Journal International*, 210(3):1739–1764, 06 2017. doi: 10.1093/gji/ggx259.

White, J. A. and Foxall, W. Assessing induced seismicity risk at CO2 storage projects: Recent progress and remaining challenges. *International Journal of Greenhouse Gas Control*, 49:413–424, 2016. doi: 10.1016/j.ijggc.2016.03.021.

Zahradník, J. and Sokos, E. *ISOLA Code for Multiple-Point Source Modeling—Review*, pages 1–28. Springer International Publishing, Cham, 2018. doi: 10.1007/978-3-319-77359-9_1.

Zang, A., Oye, V., Jousset, P., Deichmann, N., Gritto, R., McGarr, A., Majer, E., and Bruhn, D. Analysis of induced seismicity in geothermal reservoirs – An overview. *Geothermics*, 52:6–21, 2014. doi: 10.1016/j.geothermics.2014.06.005.